World Academy of Science, Engineering and Technology
International Journal of Industrial and Manufacturing Engineering
Vol:18, No:3, 2024

Tool Wear Analysis in 3D Manufactured Ti6Al4V

David Downey

***Abstract*—**With the introduction of additive manufacturing (3D printing) to produce titanium (Ti6Al4V) components in the medical, aerospace and automotive industries, intricate geometries can be produced with virtually complete design freedom. However, the consideration of microstructural anisotropy resulting from the additive manufacturing process becomes necessary due to this design flexibility and the need to print a geometric shape that can consist of numerous angles, radii, and swept surfaces. A femoral knee implant serves as an example of a 3D-printed near-net-shaped product. The mechanical properties of the printed components, and consequently, their machinability, are affected by microstructural anisotropy. Currently, finish-machining operations performed on titanium printed parts using selective laser melting (SLM) utilize the same cutting tools employed for processing wrought titanium components. Cutting forces for components manufactured through SLM can be up to 70% higher than those for their wrought counterparts made of Ti6Al4V. Moreover, temperatures at the cutting interface of 3D printed material can surpass those of wrought titanium, leading to significant tool wear. Although the criteria for tool wear may be similar for both 3D printed and wrought materials, the rate of wear during the machining process may differ. The impact of these issues on the choice of cutting tool material and tool lifetimes will be discussed.

***Keywords*—**Additive manufacturing, build orientation, microstructural anisotropy, printed titanium Ti6Al4V, tool wear.

I. Introduction

THE manufacturing of complicated geometries with free-form surfaces is attainable with 3D printing technology. According to [6], "a process of combining materials to build things from 3D model data often layer by layer, as opposed to subtractive manufacturing methodologies," is how additive manufacturing (AM) is defined. The range of engineering materials (not limited to) that can be used with this technology includes metals, ceramics, polymers, and composites. It is acknowledged that a more complex and distinctive part geometry can be produced with AM, which addresses the limitations of conventional 'subtractive' manufacturing technologies [4]. An example of such a product would be a femoral implant, from a total knee replacement system, as shown in Fig. 1.

The most widely used methods for AM of metals are laser metal deposition and powder bed fusion, which both use SLM. Metal printed parts created by AM have different microstructures, and three-dimensional multiscale structures when compared to their cast and wrought equivalents, this is attributed to the nature of the excessively fast cooling rates and directional solidification. The small melt pool generation during the AM process can locally solidify, leading to epitaxial development and the creation of grains columnar in type, due to the heat being removed through the previously created (solidified) layer. The process of repeated melting and depositing under a thermal gradient can lead to the epitaxial growth of Ti-6Al-4V, resulting in coarse primary columnar β - Ti grains. Furthermore, elevated thermal fluctuations, associated with the layer-by-layer AM process, lead to the growth of solid-state β grains. The microstructure of the AM parts can have large grains that are elongated and have textures oriented parallel to the build plate (in the build direction). However, this does not automatically mean that there is always an improved mechanical performance. To add even more complexity, other issues to be considered as part of this process include surface roughness and other surface flaws, as well as undesired porosity brought on by improper processing settings or manufacturing conditions, [19].

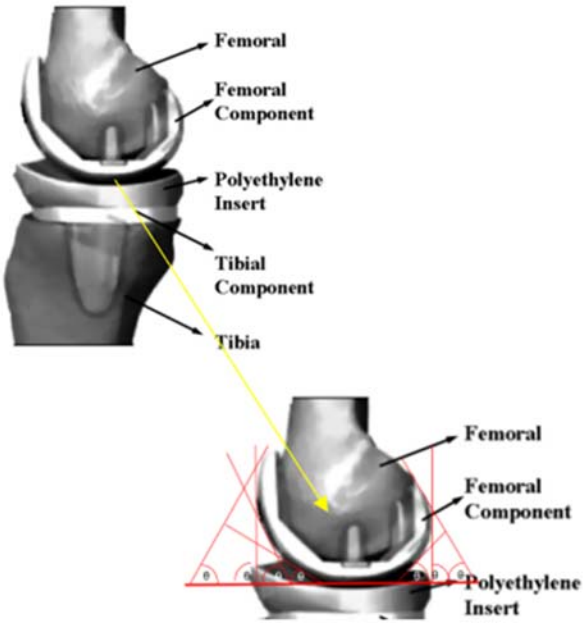

Fig. 1 Total knee replacement system and the angles that are incorporated into an AM build [9]

Reference [2] agreed that Ti-6Al-4V alloys can be processed using SLM. They opine that the deposit area can exhibit a martensitic phase, and elongated grains appear because of epitaxial development. Reference [2] determined that these grains' orientations are intimately linked with the processing conditions. When the feedstock material is exposed to an energy source, it results in the formation of liquefied pools. The

David Downey is with School of Engineering, Bernal Institute, University of Limerick, Limerick, V94 T9PX, Ireland (e-mail: 19330626@studentmail.ul.ie).

actual shape of the molten pool can be determined by the quantity of energy applied to the feedstock and substrate. The overall energy input is affected by the material's thermal diffusivity as well as the power and speed of the heat source.

According to [2], "Low speed, low power, and high thermal diffusivity cause the melt pool to take the shape of a sphere, whereas fast speed, high power, and low thermal diffusivity encourage the formation of a comet-shaped melting pool". Surface tension gradients, electromagnetic forces, and convection caused by buoyancy are other elements that affect the fusion zone's form. When the melt pool finally cools, grains with a columnar shape solidify and develop in the direction where the temperature gradient is at its highest. With the shift in the orientation of the maximum thermal gradient within the fluid, moving from the boundary of the molten pool towards the surface free of liquid, a melt pool with a rounded/spherical shape produces columnar grains that are both curved and tapered. Conversely, a melt pool shaped like a comet produces columnar grains that are straight and wide as the highest temperature gradient of the melt remains relatively constant during the solidification process. The velocity at which the energy source moves and the shape of the boundary of the liquefied area/melt pool are both geometrically linked to the pace at which the columnar grains grow. The columnar grains emerge in a parallel manner to the temperature gradient found within the liquefied zone; this happens at each melt pool boundary.

For many organizations in the medical device arena, secondary finishing operations (post-casting or 3D printing) to produce acceptable parts/products to tight tolerances are of paramount importance. In parallel to this, the machined parts need to have an acceptable level of quality and visual appearance and adhere to international GD&T standards. These operations ensure that the functionality of the part is in line with the product design intent and fulfils the market need for high-value medical device products. To fulfil this requirement, the manufacturers cannot rely on the assumption that cutting tools designed for machining wrought titanium may be a suitable solution for machining 3D-printed titanium.

II. Method

To investigate the elements that impact tool wear while machining printed titanium in current manufacturing facilities, a literature study was carried out. The microstructure of 3D printed titanium (additive produced) and how it varies from wrought titanium in bar form is of interest. The key point of interest is how this difference would affect tool wear in a production environment. While printed titanium is still considered a novel/new material, recent journal and conference publications were evaluated to gain more knowledge. The keywords used in the literature search were printed titanium Ti6Al4V, AM, tool wear, and build orientation, and from these crucial terms, a theme of microstructural anisotropy developed. The findings of the literature serve as the basis for the discussion and the new knowledge gained will help to understand why an improved cutting tool solution for machining 3D printing titanium is required.

III. Discussion

A. Microstructure & Anisotropy

SLM may be thought of as an extremely quick solidification process, where a complex macrostructure and microstructure are developed because of the significant temperature gradients produced. A modest amount of titanium powder particles are melted during the SLM process to create components made of Ti-6Al-4V. Reference [16] considered the temperature of the liquidus state of Ti-6Al-4V to be about 1650 °C, with the solidus temperature falling within the range of about 1605 °C during this process. Reference [11] expanded further when stating that the microstructure of SLM produced parts is controlled by the laser scan vector and the orientation of the build process. A fully transformed martensite α' phase is formed due to the high-temperature gradient during the printing process. Fine acicular α' grains are observed to be contained in elongated prior β grains and grow along the build direction Thus, prior β-grain orientation leads to microstructural anisotropy. It is noted that the yield and ultimate tensile strengths of the alloys created by the AM process are superior to wrought Ti-6Al-4V on average. The ductility is slightly lower than that of the wrought alloy, and there is also anisotropy related to the build direction. Moreover, there is a very minor anisotropy in the build directions that affects the yield strength and ultimate tensile strength [4].

Reference [20] also confirmed that the microstructure of SLM-produced parts is a consequence of quick solidification, and its features are associated with the orientation of thermal conduction. From Fig 2, it can be observed that there is potential for anisotropy in the mechanical properties of the material, this is evident from the clearly visible melt pool boundaries of the tracks. A more definitive melt pool boundary was observed for strategy B, due to the different laser strategies applied. It is also important to note, that, in accordance with the requirements for medical implant materials specified in [7], a 'dense/homogeneous equiaxed microstructure is required that will provide material integrity and high mechanical properties'.

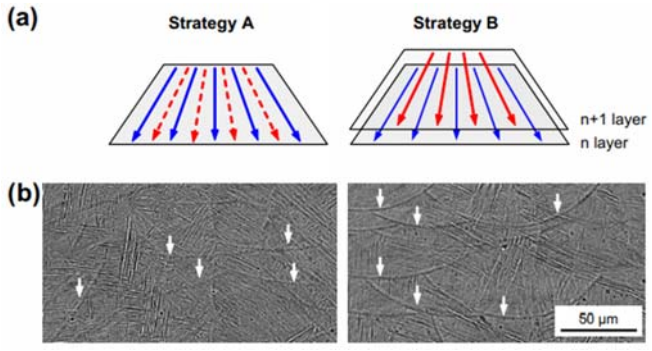

Fig. 2 SLM Scanning/build strategies for samples from Ti6Al4V powder, represented in (a) above, and SEM photos of the microstructures of specimens, white arrows indicate melt pool boundaries (b) [20]

Reference [17] recognized through testing of samples produced with different scan strategies, zigzag, unidirectional,

and cross-hatching that the grain orientation is highly scan-dependent in relation to the speed and scan strategy used, but also on the geometric shape of the part being produced. Grain orientation can be effectively controlled using the scanning strategy, and thus the microstructure texture. The unique microstructure of Ti-6Al-4V is achieved through the SLM process, which involves short interactions, a high-temperature gradient, and very localized conditions. A martensitic phase is formed due to rapid cooling, resulting in the growth of elongated grains of several hundred microns due to partial remelting of the previous layer. The orientation of the elongated particles is determined by the scanning method (and part geometry), which is determined by the local heat transfer conditions.

Reference [15] stated that Electron-Beam-Melted (EBM)-manufactured AM components have a characteristically fine structure of α/β lamellae within columnar prior-β grains which is, typical of this process. The early grain boundaries also serve as nucleation sites for the α'-Ti phase. The build orientation affects the refinement of such lamellae due to heat transfer. Conversely, a typical equiaxed microstructure is exhibited by wrought Ti-6Al-4V, which leads to the formation of an isotropic material with few defects after solidification. The annealing process used in forgings enables the coarseness of equiaxed grains with β-phase segregation at the grain boundaries. Fig. 3 shows the two different microstructures, EBM built in (a) and wrought in (b)

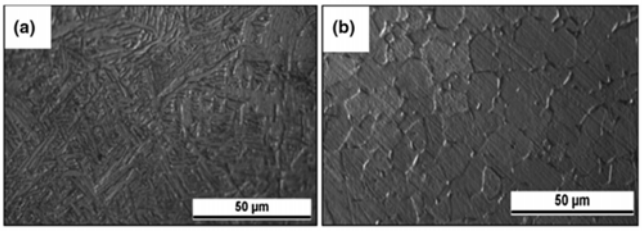

Fig. 3 Optical micrographs showing (a) lamellar microstructure of EBM builds with varying degrees of refinement and (b) equiaxed microstructure of wrought Ti-6Al-4V [15]

SLM-produced parts typically have a greater hardness/yield strength and tensile strength with a lower elastic modulus. This is evident from Table I.

TABLE I
VARIOUS FABRICATION METHODS OF TITANIUM ALLOY AND THEIR ASSOCIATED MECHANICAL PROPERTIES [8]

Fabrication Method	Hardness (HRC)	Yield Strength (MPa)	Tensile Strength (MPa)	Elastic modulus (GPa)
Wrought	31	790	872	118
EBM	35	830	914	114
SLM	41	1125	1250	94
DMLS	44	990	1095	110

Reference [1] highlights the microstructures of conventional, SLM-AB (As Built), and SLM-SR (Stress Relieved) Ti6Al4V samples in Fig. 4. The standard Ti6Al4V alloy's microstructure, as shown in Figs. 4 (a) and (b), consists of α and β phases, shown as both darker and bright regions, respectively. Figs. 4 (b) and (c), on the other hand, display the microstructure of the as-built SLM-AB sample, with α'-Martensite, formed during solidification, which is present in the grains as small needles dispersed throughout. α'-martensite can be categorized into four categories based on the size of the needles: primary, secondary, tertiary, and quaternary. The largest is primary, whereas the smallest is quaternary. The secondary martensite, which is denser and smaller than the primary, can be oriented perpendicular or at an angle of approximately 45° to the primary martensite, finally, the quaternary martensite needles are nestled within the tertiary martensite needles.

Fig. 4 (d) shows all these α'-martensite forms, where the presence of very small needles in the as-built sample structure can be attributed to the SLM process's extremely fast cooling rates. The SEM micrograph of the SLM-SR (Stress Relieved) sample's microstructure is shown in Fig. 4 (f). Apart from the α'-martensite laths, a certain amount of β phase exists due to the thermal process at a temperature of 675 °C for 1 hour, which converts some α'-martensite that was not in equilibrium into α and β phases. Since vanadium has a higher atomic weight than titanium, the small white particles inside the structure might represent the β phase. The paler shade of the β phase in comparison to the α phase is indicative of its representation. However, the martensitic structure remains the dominant feature.

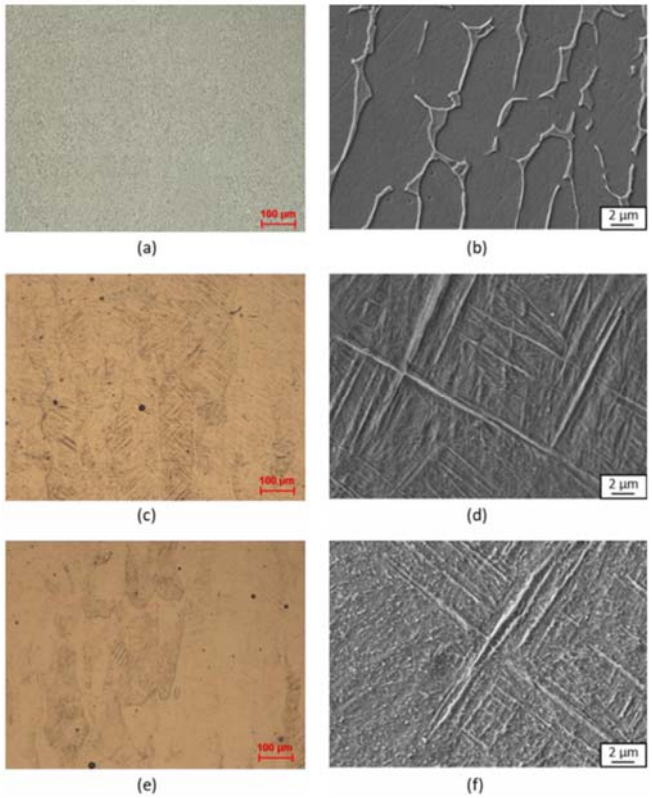

Fig. 4 Optical and SEM images representing the microstructures of the Ti6Al4V samples: (a), (b) conventional alloy; (c), (d) SLM-AB (As Built) alloy; and (e), (f) SLM-SR (Stress Relieved) alloy [1]

Reference [18] considered the mechanical properties of

untreated Ti6Al4V SLM and reference material (hot forged and subsequently mill annealed Ti6Al4V), the comparisons are shown in Fig. 5 and are listed in Table II. Even in the as-built condition, three differences are noted. Primarily, the SLM material's elastic modulus is marginally less than the reference material. This could be a result of its texture. However, the SLM material is significantly stronger than the reference material, which is a consistent observation across all materials processed by the SLM process due to the quick cooling conditions that lead to a refined microstructure. Finally, the fracture strain is substantially lower in the SLM material due to its fine lamellar structure compared to the equiaxed reference material.

Heat treatment is required to maintain as close an equivalency as possible to the wrought material (hot forged and subsequently mill-annealed Ti6Al4V). Table III summarizes the outcome of heat treatments on the SLM material. The two results from Table III that indicate the best outcomes are, number two "(2 hours at 850 °C, followed by furnace cooling) and number seven (1 hour at 940 °C, followed by air cooling and tempering for 2 hours at 650 °C and air cooling) seem to produce the best overall results" [18]. It is evident that the reaction of the reference material to the heat treatment and the impact it exerts on SLM material is very different. The yield stress does not change significantly after the different heat treatments. This is due to the α and β grains experiencing a balanced expansion at elevated temperatures, which impedes their individual growth. Consequently, the resulting grain sizes are comparable to each other after many heat treatments. [18].

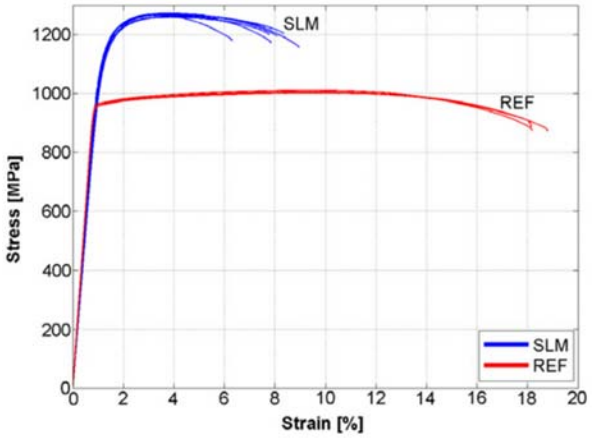

Fig. 5 Mechanical properties of untreated SLM and reference material [18]

TABLE II
MECHANICAL PROPERTIES OF UNTREATED SLM AND REFERENCE MATERIAL [18]

	E (GPa)	σ_y(MPa)	UTS (MPa)	e-fracture (%)
SLM	109.2 +/- 3.1	1110 +/- 9	1267 +/- 5	7.28 +/- 1.12
Reference	120.2 +/- 1.9	960 +/- 10	1006 +/- 10	18.37 +/- 0.88

TABLE III
MECHANICAL PROPERTIES OF SLM PRODUCED PARTS OVER VARYING HEAT TREATMENT PROCESSES [18]

Nr	T (^{0}C)	t(h)	Cooling rate	E (GPa)	σ_y(MPa)	UTS (MPa)	e-fracture (%)
	540	5	WQ	112.6 +/- 30.2	1118 +/- 39	1223 +/- 52	5.36+/- 2.02
2	850	2	FC	114.7 +/- 3.6	995 +/- 6	1004 +/- 6	12.84 +/- 1.36
3	850	5	FC	112.0 +/- 3.4	909 +/- 24	965 +/- 20	– (premature failure)
	1015	0.5	AC				
4	Followed by			114.9+/- 1.5	801 +/- 20	874 +/- 23	13.45 +/- 1.18
	843	2	FC				
5	1020	2	FC	114.7 +/- 0.9	760 +/- 19	840 +/- 27	14.06 +/- 2.53
6	705	3	AC	114.6 +/- 2.2	1026 +/- 35	1082 +/- 34	904 +/- 2.03
	940	1	AC				
7	Followed by			115.5 +/- 2.4	899 +/- 27	948 +/- 27	13.59 +/- 0.32
	650	2	AC				
	1015	0.5	AC				
8	Followed by			112.8 +/- 2.9	822 +/- 25	902 +/- 19	12.74 +/- 0.56
	730	2	AC				

According to [18], for SLM-built material, the "mechanical properties are very much dependent on the maximum heat treatment temperatures. With rising maximum temperature, σ_y and UTS decline, and the fracture strain rises because of the transformation of the fine α needles to a coarser mixture of α and β. Overall best results are obtained after 2 h at 850 °C".

The microstructure changes of parts built at different angles are not solely attributed to the AM process using Ti6Al4V powder. According to [5], it is also worth noting that, like titanium, stainless steels have different microstructures when produced by the AM process, and in particular microstructure variations were created due to differing building orientations. Fig. 6 shows the microstructure of the stainless steel, using optical microscope images. Fig. 6 (a) reveals that the sectioned view of the stainless steel produced through AM in the 0° build direction exhibits scanning tracks that are densely packed. The utilization of a 3 mm hatch spacing during the AM process led to regions of overlap between two adjoining tracks, which effectively promoted good metallurgical bonding. However, these overlapping regions were not visible in the cross-section, and only the heat-affected zone was observable between two adjacent scanning tracks.

In the stainless steel produced through AM, the shape of each layer was distinctly discernible when built at a 90° angle. As depicted in Fig. 6 (b), there were two variations of shapes present; one with rounded corners, resulting from the 'Gaussian

distribution of laser energy' [5], and the other being a straight line, formed by the path taken by the laser during scanning.

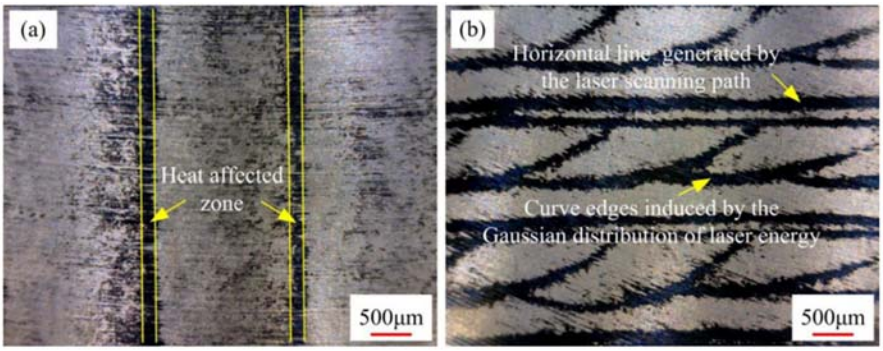

Fig. 6. Microscopic images of the stainless steel produced through AM: (a) a slice taken perpendicular to the 0◦ building direction, and (b) a section taken vertically along the 90° building orientation [5]

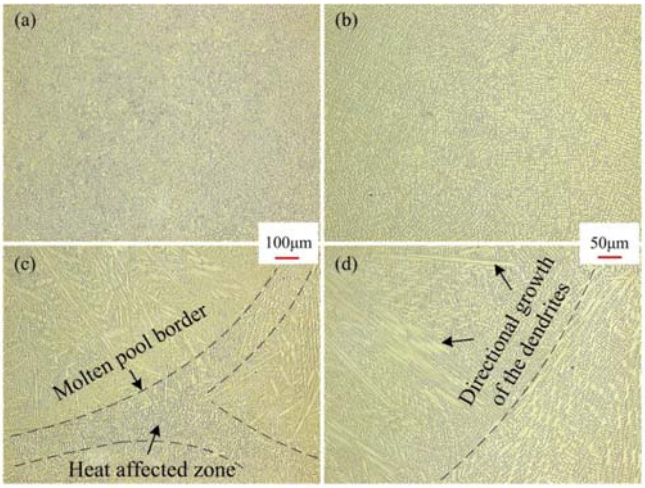

Fig. 7 Images of stainless steel produced through AM in different construction orientations: (a), (b) the 0◦ construction orientation; (c), (d) the 90◦ construction orientation [5]

Analysing Figs. 7 (a) and (b), it is apparent that the solidification texture of the stainless steel produced with a build orientation of 0° was consistent and dense, with no cavities or pores present. The enlargement of the grains did not exhibit a distinct direction, and the rapid solidification was due to the significant temperature gradient and quick rate of cooling.

In contrast, Figs. 7 (c) and (d) depict the microstructure in the vertical section, at a building direction of 90°, revealing a noticeable change in the microstructure's morphology. These two micrographs demonstrate that the solidification was primarily performed through the 'epitaxial nucleation of large dendritic grains' [5].

Throughout the AM process, a laser beam administers vast amount of energy, leading to a substantial difference in temperature between the melted pool and the region that was previously deposited. The temperature gradient along the vertical direction of the melted pool was more significant than any other direction within the pool. This caused dendrites to grow directionally, growth started from the edges of the melt pool and progressed towards the centre of the melted pool, as illustrated in Fig. 7 (d) [5].

Reference [13] conducted flat tensile tests on samples taken from longitudinal and transverse sections of a cylindrical rod, which was fabricated through SLM Ti6Al4V and wrought Ti6Al4V methods (at room temperature). The SLM bars displayed superior yield and ultimate tensile strength when compared to the wrought sample. Nevertheless, the SLM sample lacked ductility, in contrast to their wrought equivalent. This variance in the behaviour of the material can be directly attributed to the difference in their microstructure, and this affects the mechanical properties of the titanium alloy. According to [13], the mechanical properties of wrought Ti-6Al-4V are influenced by the size of the equiaxed grains, whereas in SLM Ti-6Al-4V, the properties are determined by the colony size and size of the alpha lathes. Also, the movement of dislocations is known as plastic deformation. The increased size of alpha grains in the wrought alloys permits deformation with reduced dislocations, which leads to greater yield strength, ultimate tensile strength, and reduced ductility of SLM components. The longitudinal direction of wrought titanium rods has elongated grains due to rolling, during layer-by-layer heating, the SLM rod underwent elongation of its grains, resulting in a microstructure where the grains in the transverse direction were more refined than those in the longitudinal direction. Consequently, the transverse samples exhibited greater yield strength and tensile strength compared to the longitudinal samples.

Reference [12] identified potential differences in the microstructure and microstructural variations of EBM-manufactured products. This gives emphasis to the fact that manipulation or strategic scanning strategies can alter the final microstructure and mechanical properties within limited printing dimensions in the range of 50 μm to 100 μm. When cross-referencing EBM and SLM Ti-6Al-4V manufactured parts with wrought and cast Ti-6Al-4V parts, the residual product tensile properties were analysed. The tensile strength of EBM and SLM Ti-6Al-4V manufactured parts varied to 50% greater than the wrought manufactured product. In addition to this, the changes in elongation ranged from approximately 4.4%

to 25%, and finally, the residual hardness in the EBM and SLM parts increased which is beneficial, as this has wear resistance applications that would benefit a femoral product.

IV. Tool Wear

Because the state of tool wear directly affects the cutting forces during machining and the quality of finished machined surfaces, tool wear is considered the most important component in machinability evaluation. With the extremely elevated temperatures during machining and the intense attrition at the intersection where the tool and workpiece meet, the primary wear mechanism in the machining of titanium alloys is adhesive abrasive wear. This process is largely influenced by the choice of cutting parameters. In terms of machining AMed Ti alloys, the enhanced mechanical characteristics may have a greater impact on cutting tool wear. The flank wear of cutting tools while machining SLMed Ti6Al4V can be greater than when machining wrought workpieces. According to [1], this behaviour was associated with the increased hardness of the SLMed-manufactured parts.

Reference [8] also opined that in addition to the impact of mechanical properties of AM parts, workpiece microstructure can also be a factor influencing tool wear progression. More specifically, the type of grain, their dimensions, how the grains align, and their dispersion change the intrinsic characteristics of the printed part being produced and consequently impact the level of abrasive wear experienced by the tool cutting. In a separate study by [10], an examination was conducted into the effect of additive manufactured-induced anisotropy in the material generated and its impact on cutting tool wear. Experiments were conducted in the form of milling Ti6Al4V billets produced by Laser Powder Bed Fusion (LPBF) in four different orientations 0°, 36°, 72° and 90° to the build plate. The wear results indicated that the 0^0 billet had the least wear. This is because the angle between the orientation of the α grain boundary layer (αGB) and the cutting direction became large, preventing the penetration of the work material and the formation of chip flow.

Reference [10] reaffirmed that after the AM activities, post-processing operations such as machining are essential to meet product surface finish and geometric tolerance specifications for a particular application. However, due to the printing process, the microstructure of AM parts can lead to instabilities in the machining process due to variations in cutting force, which ultimately leads to uneven tool wear and degradation of the finished parts' surface quality. Therefore, controlling how tools wear is essential to ensure repeatable high-quality machined parts, which in turn increases production efficiencies and generates long-term cost savings. Therefore, it is necessary to appreciate the effect of the anisotropic properties of AM parts on machinability, which are known to differ from wrought alloys; some studies [14], [5] have been completed on the directionality of AM microstructures based on AM parameters, The anisotropic microstructural response of AM parts in relation to machining has not been studied in finite detail and the rate at which tools wear in relation to the material anisotropy of AM produced parts is unlikely taken into consideration, when selecting cutting tool solutions for additively manufactured parts.

V. Conclusion

There is an assumption that finish-machining operations are currently performed on titanium parts, printed using SLM with the same cutting tools used to process wrought titanium components. Cutting forces for Ti6Al4V components (SLM manufactured) can be up to 70% greater than for wrought counterparts. Temperatures at the cutting interface are also higher than in wrought titanium, which can have a negative influence on tool wear. While the decisive factor for tool wear may be the same for 3D printed and wrought materials, the rate of wear throughout the machining process may differ. Knowing the impact of these issues on the choice of cutting tool material and on cutting tool lifetimes is essential for making informed decisions for engineering personnel.

According to [3], more progress is needed in studies related to drilling operations related to AM material. This lack of understanding could also apply to a knowledge shortfall concerning tapping/threading, as the two are intrinsically linked to each other via the joining of components in the aerospace industry. As a result, the absence of relevant research severely limits the implementation of AM technology across many sectors, including aerospace, medical and automotive.

Reference [17] opined that a method of identifying the scan strategy prior to machining would be beneficial in a production operations environment.

References

[1] Al-Rubaie, K.S., Melotti, S., Rabelo, A., Paiva, J.M., Elbestawi, M.A., and Veldhuis, S.C. (2020) 'Machinability of SLM-produced Ti6Al4V titanium alloy Frazier, W.E. (2014).

[2] Basak, A. and Das, S. (2016) "Epitaxy and microstructure evolution in metal additive manufacturing," Annual Review of Materials Research, 46(1), pp. 125–149. Available at: https://doi.org/10.1146/annurev-matsci-070115-031728.

[3] Dang, J., Liu, G., Chen, Y., An, Q., Ming, W., and Chen, M. (2019) 'Experimental investigation on machinability of DMLS Ti6Al4V under dry drilling process', Materials and manufacturing processes, 34(7), 749–758, available: https://doi.org/10.1080/10426914.2019.1594254.

[4] Frazier, W.E. (2014) "Metal Additive Manufacturing: A Review," Journal of Materials Engineering and Performance, 23(6), pp. 1917–1928. Available at: https://doi.org/10.1007/s11665-014-0958-z.

[5] Guo, P., Zou, B., Huang, C., and Gao, H. (2017) 'Study on microstructure, mechanical properties and machinability of efficiently additive manufactured AISI 316L stainless steel by high-power direct laser deposition', Journal of materials processing technology, 240, 12–22, available: https://doi.org/10.1016/j.jmatprotec.2016.09.005.

[6] ISO/ASTM 52900:2015(E),

[7] ISO 20160/ "Implants for surgery. metallic materials. classification of microstructures for alpha+beta titanium alloy bars" (no date). Available at: https://doi.org/10.3403/30027686.

[8] Li, G., Rahman Rashid, R., Ding, S., Sun, S., Palanisamy, S. (2022) "Machinability Analysis of Finish-Turning Operations for Ti6Al4V Tubes Fabricated by Selective Laser Melting", Metals, 12(5), 806.

[9] Li, Y., Yang, C., Zhao, H., Qu, S., Li, X., and Li, Y. (2014) 'New Developments of Ti-Based Alloys for Biomedical Applications', Materials, 7(3), 1709–1800, available: https://doi.org/10.3390/ma7031709.

[10] Lizzul, L. et al. (2020) "Influence of additive manufacturing-induced anisotropy on tool wear in end milling of ti6al4v," Tribology International, 146, p. 106200. Available at: https://doi.org/10.1016/j.triboint.2020.106200.

[11] Milton, S., Morandeau, A., Chalon, F., and Leroy, R. (2016) 'Influence of

Finish Machining on the Surface Integrity of Ti6Al4V Produced by Selective Laser Melting', Procedia CIRP, 45, 127–130, available: https://doi.org/10.1016/j.procir.2016.02.340.

[12] Murr, L., Quinones, S., Gaytan, S., Lopez, M., Rodela, A., Martinez, E., Hernandez, D., Martinez, E., Medina, F. and Wicker, R., 2009. Microstructure and mechanical behavior of Ti–6Al–4V produced by rapid-layer manufacturing, for biomedical applications. Journal of the Mechanical Behavior of Biomedical Materials, 2(1), pp.20-32.

[13] Shunmugavel, M., Polishetty, A., and Littlefair, G. (2015) 'Microstructure and Mechanical Properties of Wrought and Additive Manufactured Ti-6Al-4V Cylindrical Bars', Procedia technology, 20, 231–236, available: https://doi.org/10.1016/j.protcy.2015.07.037.

[14] Shunmugavel, M., Polishetty, A., Goldberg, M., Singh, R., and Littlefair, G. (2017) 'A comparative study of mechanical properties and machinability of wrought and additive manufactured (selective laser melting) titanium alloy – Ti-6Al-4V', Rapid prototyping journal, 23(6), 1051–1056, available: https://doi.org/10.1108/RPJ-08-2015-0105.

[15] Bruno, J., Rochman, A., and Cassar, G. (2017) 'Effect of Build Orientation of Electron Beam Melting on Microstructure and Mechanical Properties of Ti-6Al-4V', Journal of materials engineering and performance, 26(2), 692–703, available: https://doi.org/10.1007/s11665-017-2502-4.

[16] Stéphane Gorsse, Christopher Hutchinson, Mohamed Gouné & Rajarshi Banerjee (2017) Additive manufacturing of metals: a brief review of the characteristic microstructures and properties of steels, Ti-6Al-4V and high-entropy alloys, Science and Technology of Advanced Materials, 18:1, 584-610, DOI:10.1080/14686996.2017.1361305

[17] Thijs, L., Verhaeghe, F., Craeghs, T., Humbeeck, J.V., and Kruth, J.-P. (2010) 'A study of the microstructural evolution during selective laser melting of Ti–6Al–4V', Acta materialia, 58(9), 3303–3312, available: https://doi.org/10.1016/j.actamat.2010.02.004.

[18] Vrancken, B., Thijs, L., Kruth, J.-P., and Van Humbeeck, J. (2012) 'Heat treatment of Ti6Al4V produced by Selective Laser Melting: Microstructure and mechanical properties', available: https://doi.org/10.1016/j.jallcom.2012.07.022.

[19] Watanabe, Y. et al. (2019) "3D visualization of top surface structure and pores of 3D printed ti-6al-4v samples manufactured with tic heterogeneous nucleation site particles," Metallurgical and Materials Transactions A, 51(3), pp. 1345–1352. Available at: https://doi.org/10.1007/s11661-019-05597-z.

[20] Yadroitsev, I., Krakhmalev, P., and Yadroitsava, I. (2014) 'Selective laser melting of Ti6Al4V alloy for biomedical applications: Temperature monitoring and microstructural evolution', Journal of alloys and compounds, 583, 404–409, available: https://doi.org/10.1016/j.jallcom.2013.08.183.